Published in final edited form as:
Optom Vis Sci. 2012 May ; 89(5): 602–610. doi:10.1097/OPX.0b013e3182504227.

Foveal Avascular Zone and Its Relationship to Foveal Pit Shape

Toco Y. P. Chui, PhD, FAAO, **Zhangyi Zhong, PhD**, **Hongxin Song, PhD**, and **Stephen A. Burns, PhD, FAAO**
School of Optometry, Indiana University, Bloomington, Indiana

Abstract

Purpose—To investigate the retinal microvasculature at the fovea and peripheral retina in humans using the adaptive optics scanning laser ophthalmoscope (AOSLO). To examine the association of foveal avascular zone (FAZ) and foveal pit morphology.

Methods—Retinal imaging of the foveal capillary network was performed on 11 subjects (15 eyes; age range 20–54) with an AOSLO. Standard deviation maps of the AOSLO images were generated from ~10–30 frames, producing high resolution maps delineating the complete capillary distribution of the retina. Foveal pit morphology was investigated in the same subjects by using a spectral domain optical coherence tomography (SDOCT). In an additional subject, only a relatively large retinal vasculature map was obtained using AOSLO.

Results—A well demarcated FAZ was seen in 11 subjects tested with foveal capillary imaging. There was considerable individual variation in the size and shape of the FAZ. The mean FAZ area and mean FAZ effective diameter were 0.33mm^2 and 622μm, respectively. Foveal thickness was found to be negatively correlated with the FAZ effective diameter.

Conclusions—The structure of the capillary network could be evaluated in the fovea and parafovea using our approach. We find that a smaller FAZ is associated with a narrower foveal pit opening and a thicker fovea.

Keywords

foveal avascular zone; foveal pit morphology; adaptive optics scanning laser ophthalmoscope; spectral domain optical coherence tomography; retina; retinal thickness

---

The human foveola is the rod-free region of the central retina. The foveola has the maximum cone photoreceptor packing density and inner retinal layers are displaced from the foveola, resulting in the characteristic foveal pit. The absence of blood vessels and overlaying inner retinal tissue are thought to maximize the optical quality of the fovea pit by reducing light scattering. This central avascular region is known as the foveal avascular zone (FAZ).

It has been shown that the presence of an FAZ precedes the formation of the foveal pit [1]. Based on this observation, Springer and Hendrickson have developed a biomechanical model of primate foveal development, in which they suggest that the centrifugal migration of the inner retinal layer and the centripetal migration of the cone photoreceptors are

Corresponding author: Steven A. Burns, School of Optometry, Indiana University, 800 E. Atwater Ave, Bloomington, IN 47405, staburns@indiana.edu.

SUPPLEMENTAL DIGITAL CONTENT
Supplemental digital content is available online at:
Video 1: Retinal vasculature obtained at 1° superior retina - **[LWW insert link]**.
Video 2: Retinal vasculature obtained at 3° inferior retina - **[LWW insert link]**.
Video 3: Retinal vasculature obtained at 1° temporal retina - **[LWW insert link]**.

initiated by the presence of intraocular pressure and the retinal stretching during ocular growth [2–4]. Thus, the close link between retinal vascular and neural development might lead to the speculation that the size of the FAZ is highly associated with the foveal pit profile and structure.

The FAZ has been studied by researchers using various methods, such as entoptic perception [5–7], fluorescein angiography[8, 9], and adaptive optics scanning laser ophthalmoscopy (AOSLO)[10]. Previous studies have shown that the shape and size of the FAZ varied considerably in healthy subjects with a mean diameter ranging between 400 to 700μm among studies [7–9]. There is also a growing body of literature documenting the relationship between the FAZ and the foveal pit morphology delineated by optical coherence tomography [11–13]. In particular, these studies have indicated that the absence of the FAZ is associated with the absence of a foveal pit. In a recent study of the foveal shape in a normal population, the central foveal thickness was found to be inversely correlated with the size of the FAZ [14]. However, it is still not clear how the size of the FAZ is related to the foveal pit profile such as the pit width and depth.

In the present study we investigated the relationship between FAZ dimension and foveal pit morphology in 11 healthy subjects using AOSLO and spectral domain optical coherence tomography (SDOCT). The FAZ was imaged using the Indiana AOSLO and the images were processed by mapping the blood flow induced variation in reflectivity during imaging. The resulting variance maps provide an estimate of the complete capillary distribution of the human fovea, allowing us to measure the FAZ dimension. Foveal pit profile features such as foveal pit width and depth, central foveal thickness, foveal photoreceptor thickness, and the maximum retinal thickness were measured from the foveal SDOCT scans. In an additional subject, a relatively large retinal vasculature map was obtained using AOSLO.

METHODS

Subjects

Twelve healthy subjects (16 eyes; 10 Males and 2 Female; age range 20–54, mean 31, SD= ±9) participated in this study. All subjects received a complete eye examination, including a subjective refraction and fundus examination. Exclusion criteria for this study included any evidence of retinal pathology or systemic diseases. Spherical equivalent refractive errors ranged from +0.75D to −6.75D with astigmatism less than −2.00D when referenced to the spectacle plane. All subjects had best corrected visual acuity of 20/20 or better. Informed consent was obtained after a full explanation of the procedures and consequences of the study. This study protocol was approved by the Indiana University Review Board and complied with the requirements of the Declaration of Helsinki.

Procedures

Axial Length Measurement—Axial length measurement of each eye was made using an IOL Master (Carl Zeiss Meditec, Dublin, California). A mean of 5 axial length measurements was obtained for each subject. The retinal magnification differences induced by different axial lengths were factored into a calculation of linear retinal units in each subject as described previously [15].

AOSLO Instrumentation—Foveal cone photoreceptors and capillary network were investigated by using the Indiana AOSLO [16]. The light source for high resolution imaging was provided by a supercontinuum source (Fianium, Inc) with an 840nm filter. The adaptive optics control of the system was maintained using two deformable mirrors sequentially (Mirao 52D - Imagine Eyes and Boston Micromachines - BMC MEMS). Wavefront errors

were detected with a Shack Hartmann sensor operating at 18.5 Hz. The imaging raster was provided by a 10 kHz horizontal scanning galvanometer and a programmable vertical scan galvanometer. For these experiments the vertical scan was programmed to provide full frame images of 2° × 1.8° at a frame rate of 18.5Hz. Light returning from the retina passes through a confocal aperture optically conjugate to the retinal plane. The confocal aperture was 200μm for cone photoreceptor imaging and 500μm for retinal vasculature imaging, approximately 7 and 18 times the airy disc radius, respectively.

Our AOSLO system has been shown to provide a lateral resolution of better than 2.5 μm in a series of subjects, with the exact resolution dependent on the pupil size [17]. The axial resolution depends critically on the confocal aperture size, and in this study we estimate that it was on the order of 80 μm for the smaller confocal aperture and more than 150 μm for the large confocal aperture. Pupil dilation with 0.5% tropicamide was performed on 8 of the 12 subjects for AOSLO imaging, adequate data could be collected from the other 4 subject's without the need for dilation. Subject's head movements were stabilized using a chin and head rest.

AOSLO imaging acquisition: AOSLO images of the foveal capillary network were collected as short sections of sequential video frames in 11 of the 12 subjects (A total of 15 eyes). On the first subject, we tested the algorithm and the ability to stitch vascular maps together by imaging a relatively large region of the inferior retina (7.5 × 5deg). This was performed to test the ability of rapidly imaging retinal vasculature at robustly combining the images using our imaging technique. No foveal cone photoreceptors or foveal capillary network were imaged on the first subject. We next imaged the foveal avascular zone by instructing subjects (11 subjects, 15 eyes) to look around the edge and at the center of the scanning raster sequentially. Typically a single acquisition of 40 frames was sufficient to collect a data set suitable for further image processing. The entire imaging session took approximately 15 minutes per eye. All images were averaged offline and were stitched together to create foveal capillary network and retinal vasculature montages using Adobe Photoshop CS4 (Adobe Systems Inc., San Jose, CA).

AOSLO image processing - computations of vascular positions: Once image sequences were recorded, custom MATLAB routines were used to first remove the sinusoidal scanning error that arose from the resonant (horizontal) scanner. Each image was then aligned in a sequence using an approach similar to that of Stevenson [18]. In our case, starting with a template frame, each succeeding frame was aligned to the template by translation to maximize the cross-correlation between image frames. Next, we automatically matched fifty-five rectangular strips, with their long axis oriented in the direction of the fast scan (for instance, a rectangle 27 pixels tall and 143 pixels wide), to the corresponding areas of the template frame. The displacements from the template were then treated as a retinal motion time sequence. The time sequence was smoothed, and the displacement for every pixel was calculated. Each pixel was then translated according to the eye motion trace. Figures 1a and 1c show two images of the displacement corrected images at two different retinal eccentricities. These images were obtained with a 500μm confocal aperture and were further processed as described below to generate a vascular map.

Vascular mapping is based on the recognition that some of the largest changes in time in a series of retinal images arise from the change in scattering caused by the blood flow through the vasculature, which is clearly shown in Videos 1 and 2 (available at **[LWW insert link]**). This blood flow induced variation in reflectivity allows us to base estimates of vessel location on image variation. This provides in principle a "map" of the vasculature. However, to produce maps, it is also important to take into account both local variations in brightness which occur due to local changes in eye geometry or the distribution of absorbers and

scatterers, and also to remove longer term variations in overall image brightness which can occur due to subject motion, light source variations or changes in the optics of the eye which are not corrected well by the adaptive optics, especially those arising from changes in the tear film. We performed these corrections in three steps. First, each video frame was median filtered within a 3 micron region (a 3×3 kernel). Next, each image in the sequence was filtered by computing the ratio of a low pass filtered image of the retina and the image itself. This is sometimes called unsharp masking, but in this case it is actually producing a band-pass filtered contrast image. Thus, at this point in the processing the sequence of frames provides a video of the local contrast variation in the images. We then compute the standard error of each pixel intensity value in the frame over time, omitting any frames for which eye movements prevented the retinal region from being imaged in that frame. Finally, this standard error image is again median filtered to remove local variation in the standard error. This procedure results in high resolution maps of the complete capillary distribution of the human retina for the imaged region. The standard deviation maps of a set of 10 and 14 frames at the corresponding retinal vasculature of Figures 1a & 1c are shown in Figures 1b &1d, respectively. In general, the standard deviation based mapping procedure rapidly generated maps from roughly 10–30 frames of data per field (2 sec). It is of particular note that the use of the larger confocal aperture (500μm or approximately 10x the Airy disc diameter) (Figure 2b) decreased contrast of some structures relative to the more confocal images (200 μm) (Figure 2a), the decreased intensity variability with the larger aperture produced excellent vascular maps, presumably because the intensity variation arising from RBC scattering was still large.

Foveal Avascular Zone Measurements

The FAZ was delineated manually on a layer mask of the vasculature montage in Adobe Photoshop CS4 (Adobe Systems Inc, San Jose, CA). This mask was then sent to MATLAB for further computation of the FAZ area in mm^2. FAZ effective diameter (deff) was also computed as deff = 2*(sqrt(Area/π)) as described previously [10].

Infrared Fundus Imaging and Spectral Domain Optical Coherence Tomography Imaging

Infrared SLO fundus imaging and SDOCT imaging were performed on 11 of the 12 subjects (15 eyes) to obtain axial cross-sectional measurements of the retina (Spectralis HRA + OCT, Heidelberg Engineering, Heidelberg, Germany). The axial and lateral resolutions of the SDOCT were approximately 7 μm and 14 μm, respectively. A 15° × 15° (~4350 × 4350 μm) raster scan centered at the fovea consisting of 73 horizontal b-scans was obtained in each subject using the manufacturer supplied eye-tracking feature (Automatic Real Time, ART). Each b-scan was composed of 768 equally spaced a-scans. The separation between b-scans was 60μm. The horizontal foveal scan was defined as the b-scan with minimum inner retinal layer thickness at the central area among the 73 b-scans. In addition to the horizontal scans, a 15° vertical foveal b-scan was obtained by instructing the subject to look at the fixation target carefully and steadily. To reduce speckle noise, each b-scan was created by averaging 20 frames. All fundus images and b-scan images were exported as tiff files for further image processing.

SDOCT Image Processing—On the horizontal and vertical foveal b-scans, the anterior boundary of RPE was flattened using a custom MATLAB program (Mathworks, Inc., Natick, Massachusetts). First, the anterior boundary of the RPE layer was identified manually and read into MATLAB. The program then applied a polynomial flattening algorithm on individual SDOCT images by sliding each pixel column vertically. Second, the boundary of the inner limiting membrane (ILM) and the border between the outer nuclear layer and the outer plexiform layer (ONL/OPL) were identified automatically similar to the method of Dubis et al. [19]. Figure 3 shows the parameters obtained from the foveal b-scans.

Central foveal thickness (CFT) was defined as the minimum distance between the first signal from the ILM and the signal from the anterior boundary of the RPE at the fovea. Foveal photoreceptor thickness (FPT) was defined as the maximum distance between the first signal from the ONL/OPL and the signal from the anterior boundary of the RPE at the fovea. Two horizontal lines were extended from the highest point of the parafoveal crests on the temporal and nasal retina (horizontal foveal scan) or inferior and superior retina (vertical foveal scan). These horizontal lines were parallel to the flattened RPE layer. Foveal pit depth (FD) was then measured from the deepest point of the pit to the mean of the horizontal lines over the pit. Foveal width at half foveal pit depth (FWHM) was then computed. Crest to crest (CC) distance was measured from the highest point of the parafoveal crests on each side of the foveola. Max. retinal thickness (MaxRT) was defined as mean of the retinal thickness at the parafoveal crest on each side of the foveola.

Statistical Analysis

Statistical analysis was performed on 11 subjects who had tested with both AOSLO and SDOCT imaging. Data were averaged in individual subjects who had both eyes tested (4 subjects). Pearson's correlation and statistical significance were computed on the FAZ and SDOCT parameters using IBM SPSS software (SPSS 19, Chicago, IL).

RESULTS

The imaging approach was able to produce maps of the vasculature rapidly and with a fairly consistent contrast as seen in Figure 4. In this map complete connections from arterioles to venules are apparent. While occasional frames have lower contrast or frame artifact as visible in the upper right corner, the overall quality is sufficient for determining vascular structure with at least the central 10 degree of the retina.

FAZ Dimension

We imaged the microvasculature surrounding the fovea for approximately 15 minutes per eye. A well demarcated FAZ was seen in all 15 eyes tested with the foveal capillary network imaging. There was considerable individual variation in the size and shape of the FAZ. The mean FAZ area was 0.33mm^2 (range 0.04–0.66mm^2; SD±0.19), and the mean FAZ effective diameter was 622μm (range 231–916μm; SD±203). Both eyes were examined in 4 of the 11 subjects. The mean difference in the FAZ effective diameter between the two eyes was 8.75% (range 4–11%; SD±3.3). No statistical significance was found on the difference in FAZ diameter between 2 eyes (Paired T test, $p>0.05$).

Figure 5 shows an example of the foveal capillary montages subtending approximately 3.5×3° in both eyes of a single subject. The FAZs of the two eyes have different sizes and shapes. The arterioles and venules in both montages were labeled after comparing them to those seen in the corresponding wide field fundus pictures. Three subjects had relatively small FAZ area (0.04 mm^2, 0.10 mm^2, and 0.16 mm^2)when compared to the average (0.33 mm^2). Figure 6 shows the foveal capillary montages and the horizontal and vertical foveal SDOCT scans collected from a 57-year-old male, who had capillaries running close to the foveola in both eyes. In these eyes the foveal SDOCT scans revealed an overall thickening of the inner retinal layer and outer nuclear layer at the foveola, with mean CFT and the mean FPT were 282.50μm and 232.39μm, respectively.

The means and standard deviations of the SDOCT parameters are shown in Table 1. The FD and CC distance, but not the FWHM measured by SDOCT were correlated with FAZ area as shown in Figure 7. The regression slopes of the CC distance and FD had a Pearson correlation coefficients of 0.76 (p-value = 0.003, 1-tailed) and 0.66 (p-value = 0.014, 1-

tailed), respectively. As shown in Figure 8a, the CFT and FPT were found to be negatively correlated with the FAZ effective diameter with the Pearson correlation coefficients of −0.80 (p-value = 0.002, 1-tailed) and −0.72 (p-value =0.006, 1-tailed), respectively (black regression lines). No statistical significance was found in MaxRT. In Figure 8b, we show results where subjects were divided into two groups: Group 1 with FAZ less than the sample mean of 620 μm (n=4) and Group 2 with FAZ greater than the sample mean of 620 μm (n=7). This division was performed to examine whether the correlation of FAZ with FPT was dominated by the 4 individuals with a very small FAZ. No statistical significance was found in MaxRT in both groups. The regression slopes of the CFT had a Pearson correlation coefficients of −0.91 (p-value = 0.04, 1-tailed) and 0.80 (p-value =0.015, 1-tailed) in Group 1 and Group 2, respectively. The regression slope of the FPT in Group 2 was found statistically significant with a Pearson correlation coefficient of 0.70 (p-value = 0.04, 1-tailed). However, no statistical significance was found in FPT in Group 1.

DISCUSSION

The present study quantitatively examined the association of the FAZ dimensions and the foveal pit profile and structure as predicted by a current model of foveal development [2, 4, 20] in normal eyes. Our findings of FAZ dimension [7, 8, 10, 21, 22] and foveal shape morphology [14] are in close agreement with previous studies. Also in agreement with previous studies, we found a large individual variation of the FAZ size and shape in healthy retinas.

Prior studies have emphasized that even when the FAZ is small, the subjects often have normal vision [23, 24]. However, a small FAZ could potentially impact more than visual acuity and cone packing density. It has been shown that the presence of a FAZ precedes the formation of the foveal pit during development [1]. Based on this observation, a model of foveal pit development [2, 4, 20] suggests that the presence of intraocular pressure and retinal stretching during ocular growth widens the foveal pit because the FAZ is more deformable than the adjacent vascularized retina, and is therefore susceptible to stretching resulting from eye growth and intraocular pressure [2–4]. This model also suggests that retinal stretching during ocular growth promotes centripetal migration of the outer retinal layers and the centrifugal migration of the inner retinal layer. Thus, in its simplest form the model can be interpreted to predict that FAZ width (CC and FWHM) is positively correlated with the foveal photoreceptor thickness (FPT) and perifoveal retinal thickness (MaxRT). The present study does find that retinas with small FAZ (<620 μm) have a shallow fovea pit, when compared with those with a relatively larger FAZ, and they also have slightly larger foveal photoreceptor thickness (Figure 7 and 8) which includes not only the cone cell bodies but also glial cells and photoreceptor axons. Because of this, the thickening of the outer retina layers is not an indication of higher photoreceptor density, since the same type of thickening of the outer retina can be seen in localized damage to the retina. [25, 26]

Likewise, we also found a thickened CFT in eyes with small FAZ due to the incomplete regression of the inner retinal layer. In contrast, our finding of the MaxRT remains relatively constant with increasing FAZ diameter. This suggests that the MaxRT is less associated to the FAZ dimension probably due to remodeling of the inner retinal layer during foveal pit formation.

Thus, it is reasonable to speculate that a small FAZ diameter with the presence of capillaries and astrocytes close to the foveola retarded the centrifugal migration of the inner retinal layers during development but did not necessarily promote the centripetal migration of the outer retinal layers. Another possibility is that the thickened photoreceptor layer in individuals with smaller FAZ areas arises from mechanical considerations perhaps due to an

interaction of glial and mechanical factors. Of particular note, although the presence of overlaying inner retinal layer, thickened FPT, and small FAZ have been reported previously in eyes with retinopathy of prematurity [13, 27, 28], no history of preterm birth was reported by our subjects. Also shown in Figure 7, CC distance and FD are positively correlated with the FAZ effective diameter, suggesting a larger FAZ effective diameter is associated with a wider and deeper foveal pit. However it is noteworthy that the majority of the correlation is arising from eyes with relatively small FAZ sizes. This is unlikely to be a result of the relatively small sample since our SDOCT data on the foveal diameter are in agreement with recent studies [13, 19], as is our estimate of the FAZ area [7, 8, 10, 21, 22].

CONCLUSIONS

We have used the AOSLO along with a new image processing approach to systematically image the foveal capillary network and peripheral retinal vasculature, allowing direct and noninvasive assessment of the retinal microvasculature *in vivo*. Smaller FAZ is associated with a narrower foveal pit opening and a larger foveal thickness (both CFT and FPT). As suggested by the finding of thickened FPT with decreasing FAZ diameter, the present study also agrees with a previous study that foveal cone migration occurs even when the foveal pit is absent [24]. Application of our findings improves our ability to understand how foveal avascular zone associated with foveal pit morphology in healthy human eyes. Our findings are important in helping researcher understanding the development of foveal pit and foveal fine structure. This technique may be useful in detecting and monitoring retinal microvasculature abnormality in retinal diseases *in vivo*.

Supplementary Material

Refer to Web version on PubMed Central for supplementary material.

Acknowledgments

The authors would like to thank the anonymous reviewers for their valuable comments and suggestions. This work was supported by NIH grants R01-EY14375, R01-EY04395, and P30EY019008 to SAB.

References

1. Provis JM, Sandercoe T, Hendrickson AE. Astrocytes and blood vessels define the foveal rim during primate retinal development. Invest Ophthalmol Vis Sci. 2000; 41:2827–36. [PubMed: 10967034]
2. Springer AD, Hendrickson AE. Development of the primate area of high acuity. 1. Use of finite element analysis models to identify mechanical variables affecting pit formation. Vis Neurosci. 2004; 21:53–62. [PubMed: 15137581]
3. Springer AD, Hendrickson AE. Development of the primate area of high acuity. 2. Quantitative morphological changes associated with retinal and pars plana growth. Vis Neurosci. 2004; 21:775–90. [PubMed: 15683563]
4. Springer AD, Hendrickson AE. Development of the primate area of high acuity, 3: temporal relationships between pit formation, retinal elongation and cone packing. Vis Neurosci. 2005; 22:171–85. [PubMed: 15935110]
5. Bradley A, Zhang H, Applegate RA, Thibos LN, Elsner AE. Entoptic image quality of the retinal vasculature. Vision Res. 1998; 38:2685–96. [PubMed: 12116711]
6. Yap M, Gilchrist J, Weatherill J. Psychophysical measurement of the foveal avascular zone. Ophthalmic Physiol Opt. 1987; 7:405–10. [PubMed: 3454917]
7. Bird AC, Weale RA. On the retinal vasculature of the human fovea. Exp Eye Res. 1974; 19:409–17. [PubMed: 4426347]

8. Bresnick GH, Condit R, Syrjala S, Palta M, Groo A, Korth K. Abnormalities of the foveal avascular zone in diabetic retinopathy. Arch Ophthalmol. 1984; 102:1286–93. [PubMed: 6477244]
9. Laatinainen L, Larinkari J. Capillary-free area of the fovea with advancing age. Invest Ophthalmol Vis Sci. 1977; 16:1154–7. [PubMed: 924747]
10. Tam J, Martin JA, Roorda A. Noninvasive visualization and analysis of parafoveal capillaries in humans. Invest Ophthalmol Vis Sci. 2010; 51:1691–8. [PubMed: 19907024]
11. Murakami T, Nishijima K, Sakamoto A, Ota M, Horii T, Yoshimura N. Foveal cystoid spaces are associated with enlarged foveal avascular zone and microaneurysms in diabetic macular edema. Ophthalmology. 2011; 118:359–67. [PubMed: 20656355]
12. Walsh MK, Goldberg MF. Abnormal foveal avascular zone in nanophthalmos. Am J Ophthalmol. 2007; 143:1067–8. [PubMed: 17524786]
13. Hammer DX, Iftimia NV, Ferguson RD, Bigelow CE, Ustun TE, Barnaby AM, Fulton AB. Foveal fine structure in retinopathy of prematurity: an adaptive optics Fourier domain optical coherence tomography study. Invest Ophthalmol Vis Sci. 2008; 49:2061–70. [PubMed: 18223243]
14. Tick S, Rossant F, Ghorbel I, Gaudric A, Sahel JA, Chaumet-Riffaud P, Paques M. Foveal shape and structure in a normal population. Invest Ophthalmol Vis Sci. 2011; 52:5105–10. [PubMed: 21803966]
15. Chui TY, Song H, Burns SA. Individual variations in human cone photoreceptor packing density: variations with refractive error. Invest Ophthalmol Vis Sci. 2008; 49:4679–87. [PubMed: 18552378]
16. Ferguson RD, Zhong Z, Hammer DX, Mujat M, Patel AH, Deng C, Zou W, Burns SA. Adaptive optics scanning laser ophthalmoscope with integrated wide-field retinal imaging and tracking. J Opt Soc Am (A). 2010; 27:A265–77.
17. Zou W, Qi X, Burns SA. Woofer-tweeter adaptive optics scanning laser ophthalmoscopic imaging based on Lagrange-multiplier damped least-squares algorithm. Biomed Opt Express. 2011; 2:1986–2004. [PubMed: 21750774]
18. Stevenson, SB.; Roorda, A. Correcting for miniature eye movements in high resolution scanning laser ophthalmoscopy. In: Manns, F.; Soderberg, P.; Ho, A., editors. Ophthalmic Technologies XV. Proceedings of the Society of Photo-Optical Instrumentation Engineers (SPIE). Vol. 5688. Bellingham, WA: SPIE Press; 2005. p. 145-51.
19. Dubis AM, McAllister JT, Carroll J. Reconstructing foveal pit morphology from optical coherence tomography imaging. Br J Ophthalmol. 2009; 93:1223–7. [PubMed: 19474001]
20. Springer AD. New role for the primate fovea: a retinal excavation determines photoreceptor deployment and shape. Vis Neurosci. 1999; 16:629–36. [PubMed: 10431912]
21. Popovic Z, Knutsson P, Thaung J, Owner-Petersen M, Sjostrand J. Noninvasive imaging of human foveal capillary network using dual-conjugate adaptive optics. Invest Ophthalmol Vis Sci. 2011; 52:2649–55. [PubMed: 21228372]
22. Arend O, Wolf S, Jung F, Bertram B, Postgens H, Toonen H, Reim M. Retinal microcirculation in patients with diabetes mellitus: dynamic and morphological analysis of perifoveal capillary network. Br J Ophthalmol. 1991; 75:514–8. [PubMed: 1911651]
23. Yu PK, Balaratnasingam C, Morgan WH, Cringle SJ, McAllister IL, Yu DY. The structural relationship between the microvasculature, neurons, and glia in the human retina. Invest Ophthalmol Vis Sci. 2010; 51:447–58. [PubMed: 19643967]
24. Marmor MF, Choi SS, Zawadzki RJ, Werner JS. Visual insignificance of the foveal pit: reassessment of foveal hypoplasia as fovea plana. Arch Ophthalmol. 2008; 126:907–13. [PubMed: 18625935]
25. Chui TY, Thibos LN, Bradley A, Burns SA. The mechanisms of vision loss associated with a cotton wool spot. Vision Res. 2009; 49:2826–34. [PubMed: 19703485]
26. Gomez ML, Mojana F, Bartsch DU, Freeman WR. Imaging of long-term retinal damage after resolved cotton wool spots. Ophthalmology. 2009; 116:2407–14. [PubMed: 19815278]
27. Mintz-Hittner HA, Knight-Nanan DM, Satriano DR, Kretzer FL. A small foveal avascular zone may be an historic mark of prematurity. Ophthalmology. 1999; 106:1409–13. [PubMed: 10406630]

28. Wang J, Spencer R, Leffler JN, Birch EE. Critical period for foveal fine structure in children with regressed retinopathy of prematurity. Retina. 2012; 32:330–9. [PubMed: 21900854]

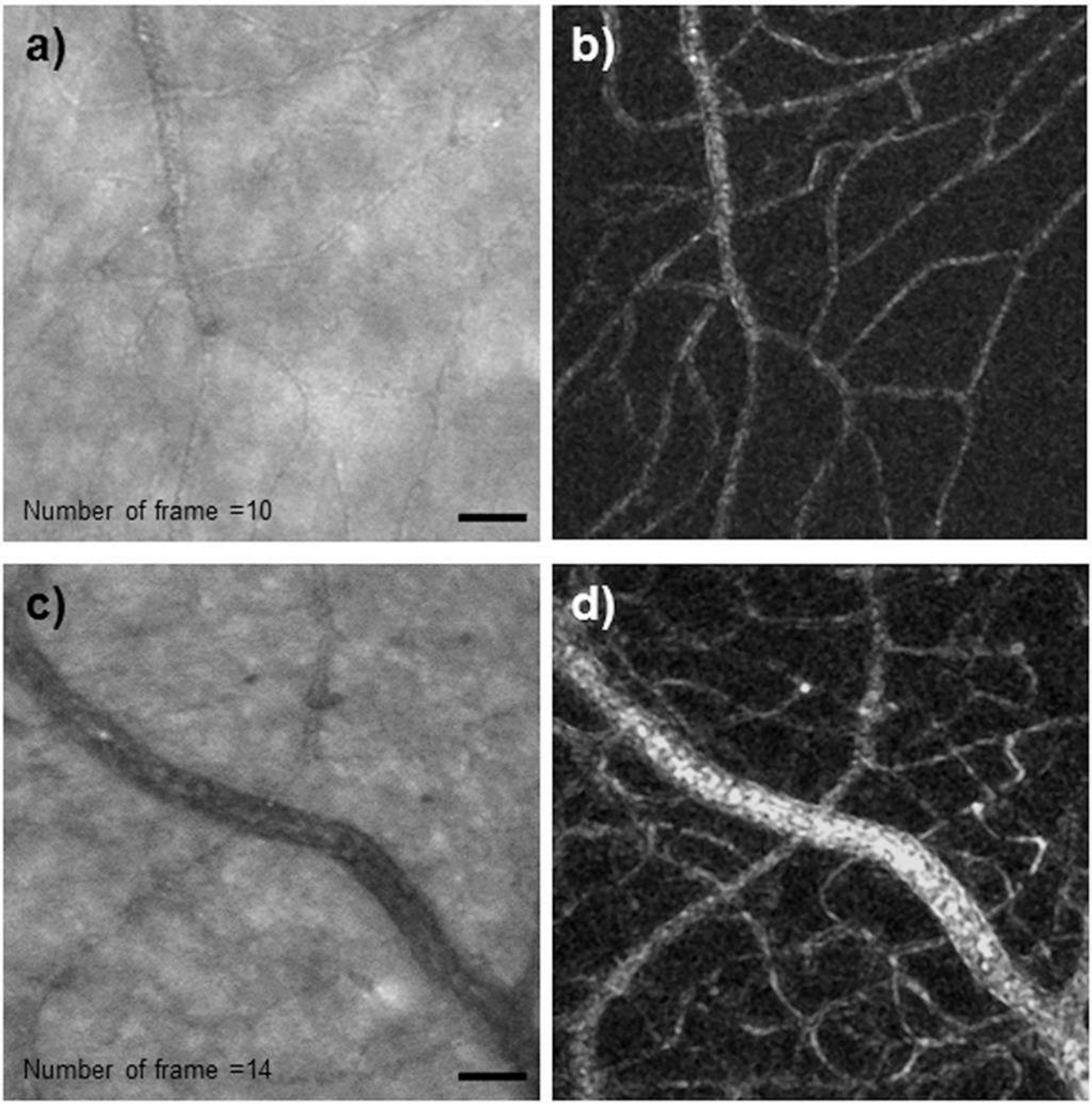

Figure 1.
Registered video sequences of retinal vasculature. Videos were obtained at **(a)** 1° superior retina (Video 1 available at **[LWW insert link]**) and **(c)** 3° inferior retina (Video 2 available at **[LWW insert link]**). The variance maps of the corresponding images are shown in **(b)** and **(d)**. In general each capillary can be found in the processed images on the right column. Scale bar = 50 μm.

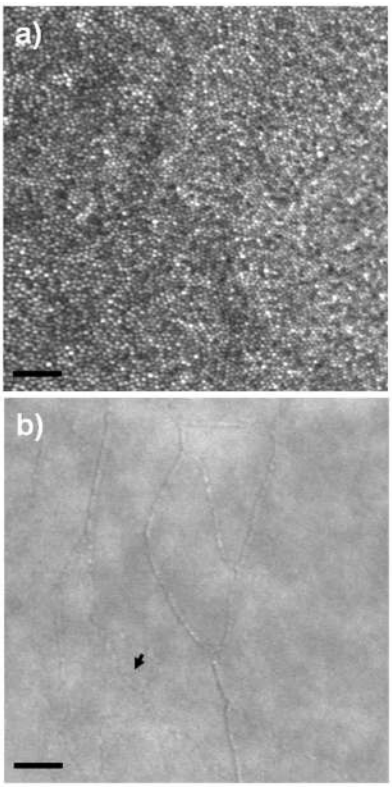

Figure 2.
Videos with 16 registered frames obtained at 1° temporal retina showing **(a)** cone photoreceptor using a 200μm confocal aperture and **(b)** retinal capillary using a 500μm confocal aperture. Arrow indicates individual RBCs flowing inside a capillary. Scale bar = 50μm. (Video 3 available at **[LWW insert link]).**

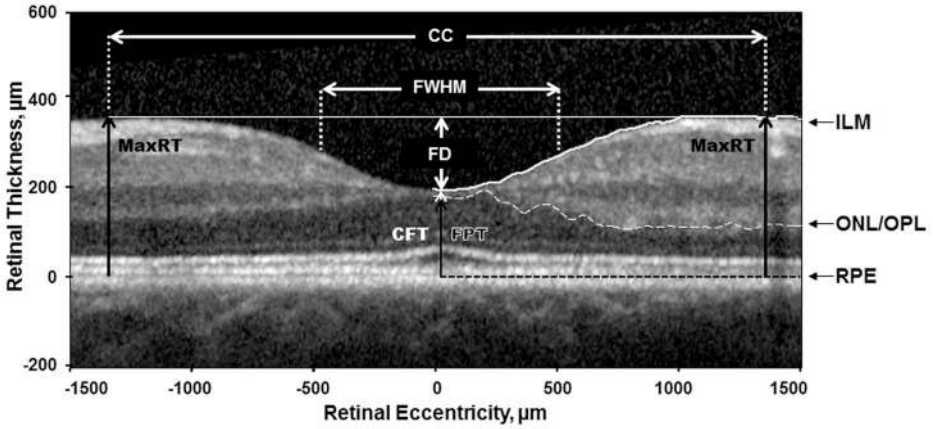

Figure 3.

Parameters obtained from the horizontal and vertical foveal SDOCT scans. **ILM –** Border of the inner limiting membrane (white solid line); **ONL/OPL** – Border of the outer nuclear layer and the outer plexiform layer (white dashed line); **RPE** – Anterior boundary of the retinal pigment epithelium (black dashed line). Segmentation lines on the left side have been removed for better visualization of the image. **MaxRT –** Maximum retinal thickness; **CFT –** Central foveal thickness; **FPT –** Foveal photoreceptor thickness.

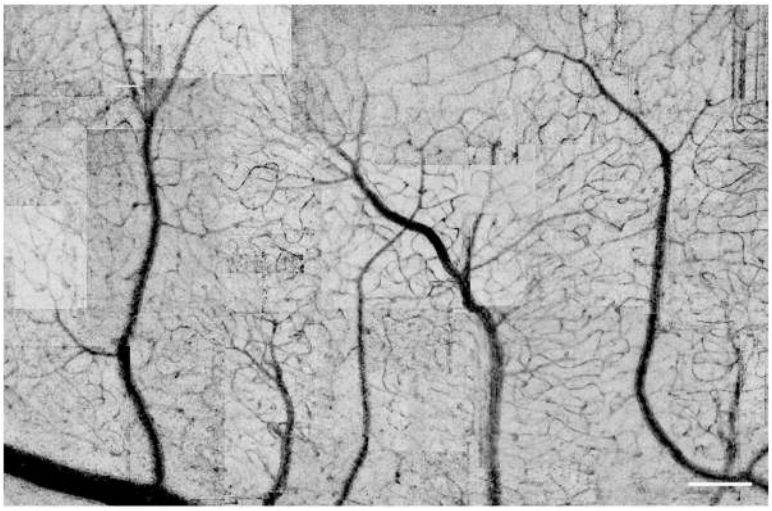

Figure 4.
A montage of images from the vascular mapping technique. In this image the regions of high variance are shown as dark to improve visibility of the vascular tree. Scale bars = 200 μm.

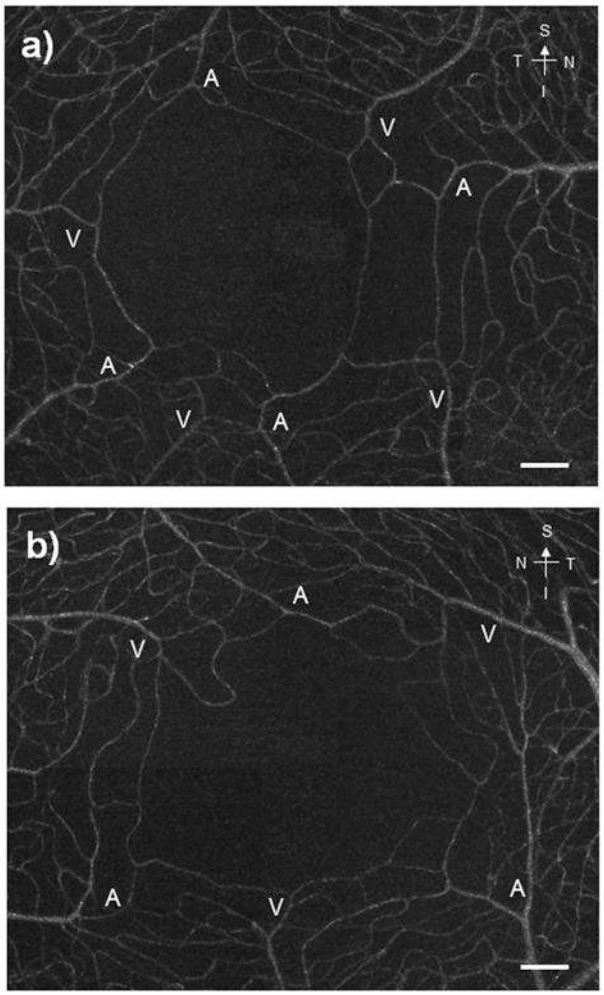

Figure 5.
foveal vasculature maps in both eyes from the same subject. Arterioles and venules are labeled as "A" and "V", respectively. In these montages, capillaries connecting the arterioles and the venules are clearly seen. Scale bars = 100 μm.

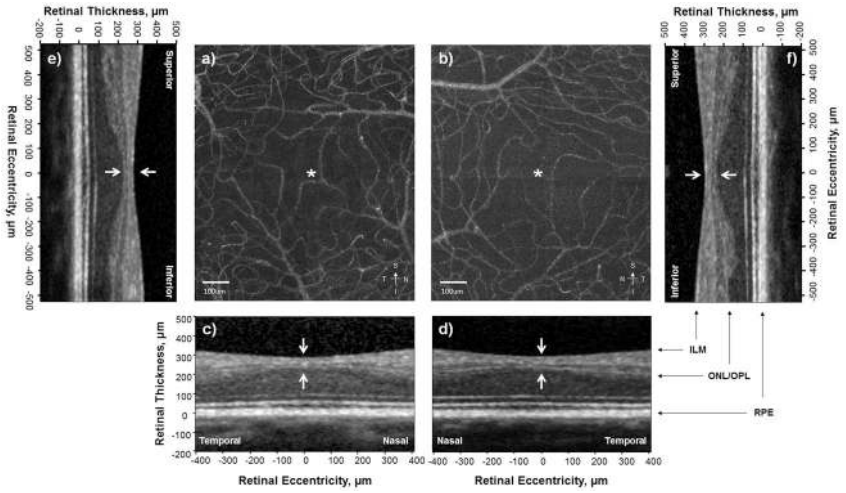

Figure 6.

(a & b) Foveal capillary montages collected from a 57-year-old male, who has capillaries running close to the foveola. Asterisks indicate the projection of the subject's fixation point on the retina. **(c–f)** Horizontal and vertical foveal b-scans of the corresponding foveal capillary montages on a & b. SDOCT scans reveal an overall thickening of the retina at the foveola as indicated by the white arrows.

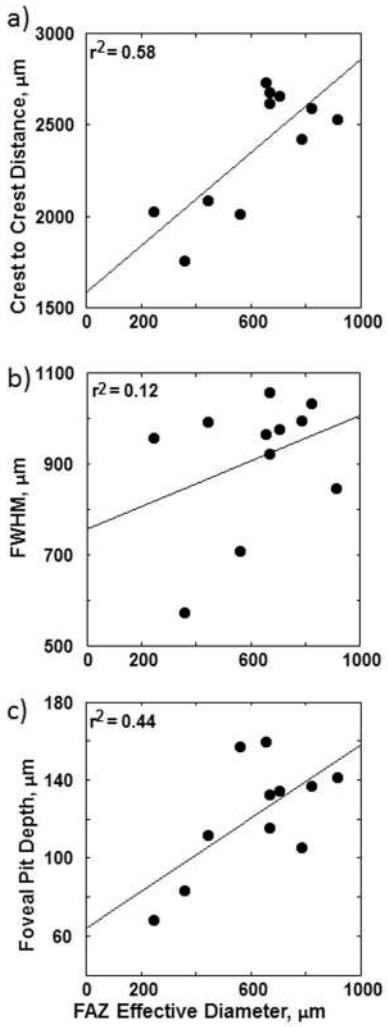

Figure 7.

(a) Mean crest to crest (CC) distance, **(b)** mean full width half maximum (FWHM), and **c)** mean foveal depth (FD) obtained from the horizontal and vertical foveal b-scans as a function of FAZ effective diameter. Linear regressions to the data are showed by the solid lines. Only the regression slopes to the crest to crest distance and foveal pit depth are statistically significant with $p<0.05$.

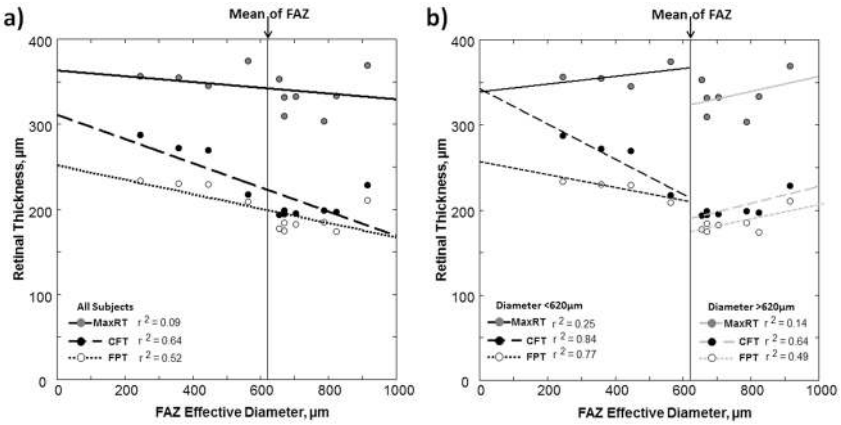

Figure 8.

Relationship between retinal layer thicknesses and FAZ effective diameter. The solid lines are the linear regression of the mean maximum retinal thickness (MaxRT) obtained from both horizontal and vertical foveal b-scans. The dashed lines are the linear regression of the mean central foveal thickness (CFT). The dotted lines are the linear regression of the mean foveal photoreceptor thickness (FPT). **(a)** Regression lines represent correlations for all subjects**. (b)** Regression lines represent correlations in subjects with FAZ diameter less than (black lines) or greater than (gray lines) the sample mean of 620 μm.

Table 1

Mean and SD of the parameters measured from AOSLO and SDOCT images.

Parameters	Mean ± SD
FAZ area	0.33mm^2 ±0.19
FAZ effective diameter	622μm ±203
Central foveal thickness (CFT)	223μm ±36
Foveal photoreceptor thickness (FPT)	199μm ±24
Maximum retinal thickness (MaxRT)	343μm ±23
Crest to crest distance (CC)	2374μm ±340
Full width half maximum (FWHM)	912μm ±148
Foveal pit depth (FD)	122μm ±29